organics

MDPI

Communication

Design, Synthesis, and Drug-Likeness Assessment of Azole-Functionalized Hydrazone Derivatives: Towards Antimicrobial Activity

Juozas Kiltinavičius [1], Kristina Kantminienė [2,*], Ilona Jonuškienė [1] and Ingrida Tumosienė [1]

[1] Department of Organic Chemistry, Kaunas University of Technology, Radvilėnų pl. 19, 50254 Kaunas, Lithuania; juozuxas12@gmail.com (J.K.); ilona.jonuskiene@ktu.lt (I.J.); ingrida.tumosiene@ktu.lt (I.T.)

[2] Department of Physical and Inorganic Chemistry, Kaunas University of Technology, Radvilėnų pl. 19, 50254 Kaunas, Lithuania

* Correspondence: kristina.kantminiene@ktu.lt

Abstract

Reaction of 5-oxo-1-(4-(phenylamino)phenyl)pyrrolidine-3-carbohydrazide with selected aldehydes and ketone provided novel hydrazone derivatives bearing azole moieties: pyrazole, pyrrole, and indole. The drug likeness of the newly synthesized compounds and their physicochemical characteristics were examined to fit Lipinski's Rule of Five. *N*-(2,5-dimethyl-1*H*-pyrrol-1-yl)-5-oxo-1-(4-(phenylamino)phenyl)pyrrolidine-3-carboxamide (**5**) exhibited the most favorable overall ADMET profile, combining compliance with key physicochemical requirements for antimicrobial activity with superior solubility and reduced predicted hepatotoxicity and nephrotoxicity. Despite generally elevated plasma protein binding across the series, this compound provided the most advantageous balance between permeability, systemic exposure, and safety.

Keywords: 5-oxopyrrolidine; diphenylamine; in silico; Lipinski's rule of five

1. Introduction

Increasing antimicrobial resistance (AMR) continues to pose a profound global health threat as it threatens ability of modern healthcare systems to effectively manage infectious diseases [1]. The World Health Organization (WHO) has listed AMR as one of the top 10 threats to human health [2]. Traditional antibiotics are losing efficacy as microorganisms acquire resistance through drug-degrading enzymes, target modifications, and efflux mechanisms, making the development of new antimicrobial agents, capable of overcoming increasingly drug-resistant bacterial and fungal pathogens, an urgent priority [3].

Hydrazone derivatives are among intensively studied heterocyclic scaffolds in antimicrobial drug discovery due to their versatile azomethine (–NH–N=CH–) linkage, which plays a critical role in biological recognition and metal coordination. Several prescribed drugs, including isoniazid, an antibiotic used to treat tuberculosis [4], and nifuroxazide, an antibiotic indicated in the treatment of gastrointestinal infections [5], contain a hydrazide–hydrazone functionality. Hydrazone derivatives are attractive compounds in medicinal chemistry because it is easy to change their lipophilicity, total charge and planarity by proper choice of the main core and/or substituents, resulting in diverse biological activities including antioxidant, antimicrobial, antitubercular, anticancer, anti-inflammatory,

Academic Editors: Alessandro Scarso and Wim Dehaen

Received: 23 March 2026
Revised: 8 May 2026
Accepted: 14 May 2026
Published: 18 May 2026

and antidiabetic effects, with hybrids like isatin– or pyridine–hydrazones enhancing potency via moiety synergy [6–11]. They also contain a site of protonation–deprotonation and possess the NH group that can participate in H-bonding [12]. Hydrazide–hydrazone compounds demonstrate potent antibacterial and antifungal activities, often outperforming conventional antibiotics through topoisomerase inhibition, efflux pump blockade, biofilm disruption, ROS induction, and increased metal chelation [12–15].

The most common route in synthesis of hydrazones is the condensation of a carboxylic acid hydrazide with an appropriate aldehyde or ketone [16]. This nucleophilic addition reaction involves the attack of the terminal amino group of the hydrazide on the carbonyl carbon of the aldehyde or ketone, followed by the elimination of a water molecule to form a stable C=NC=N double bond. The resulting hydrazone bond is stabilized by the delocalization of electrons, i.e., it is facilitated by the electronegativity of the hydrazide carbonyl oxygen. The synthesis reaction of hydrazones is commonly performed in organic solvents like ethanol or methanol, often under reflux conditions, and can be accelerated by the presence of acid catalysts or through structural tuning, such as the inclusion of neighboring acid/base groups that enhance reaction kinetics at physiological pH [17].

5-Oxopyrrolidine (pyrrolidin-2-one) derivatives constitute a versatile class of bioactive molecules, owing to their five-membered lactam structure, which serves as a versatile scaffold in medicinal chemistry often enhancing biological activity through its rigid cyclic structure and hydrogen bonding capabilities [18]. In drug discovery, the 5-oxopyrrolidine core has been highlighted for its synthetic flexibility and pharmacophore richness, contributing to the development of new therapeutic agents with activities ranging from cytotoxic effects on cancer cell lines to inhibition of bacterial growth and modulation of neurological pathways [18]. Studies have demonstrated that structural modification of the 5-oxopyrrolidine skeleton, particularly via substitution at the nitrogen or carbon positions, can significantly influence antimicrobial and anticancer efficacy, further underscoring the scaffold's importance in designing next-generation multifunctional drug candidates [18,19].

Diphenylamine is a flexible skeleton for drug development [20]. Diphenylamine derivatives have been reported to possess important biological properties, including anticancer, antimalarial, and antimicrobial activity [21,22]. 2-(Benzylidenehydrazinyl)-*N*,*N*-diphenylacetamide derivatives have shown significant activity against bacterial and fungal strains indicating the potential of diphenyl-hydrazine derivatives as antimicrobial agents [23].

Azole moieties, particularly pyrrole, pyrazole, and indole fragments, are important pharmacophores in antimicrobial agents due to their ability to mimic nucleobases, chelate metals, and disrupt microbial enzymes or membranes [19,24,25]. Pyrazole derivatives exhibit broad-spectrum antibacterial activity through DNA gyrase inhibition, with *N*-substituted pyrazoles showing potent effects against *S. aureus* and *E. coli* (MIC 4–16 μg/mL), often enhanced by hybridizing with other heterocycles [26]. Indole fragments, prevalent in natural antifungals like gliotoxin derivatives, interfere with ergosterol biosynthesis and biofilm formation, delivering antifungal efficacy against *Candida* species (MIC 3–12 μg/mL) comparable to fluconazole [27].

Chemical absorption, distribution, metabolism, excretion, and toxicity (ADMET), play key roles in drug discovery and development. A high-quality drug candidate should not only have sufficient efficacy against the therapeutic target, but also show appropriate ADMET properties at a therapeutic dose. A lot of in silico models are hence developed for prediction of chemical ADMET properties [28]. There is no universal ADMET range that guarantees strong antimicrobial activity due to antimicrobial potency being dependent on target interaction and bacterial penetration mechanisms. However, there are empirically

favourable ranges of physicochemical and ADMET-related properties that are commonly associated with successful antibacterial drugs—especially for small-molecule antibiotics.

When assessing the drug likeness of newly synthesized compounds, their physicochemical characteristics are examined to fit Lipinski's Rule of Five (RO5). It is worth mentioning that although classical drug-likeness criteria (e.g., Lipinski's RO5) provide a general framework, many approved antibiotics deviate from these rules. Nevertheless, empirical ranges for key physicochemical and pharmacokinetic parameters have emerged from analyses of successful antibacterial agents.

With antibiotic resistance escalating worldwide, hydrazone-based molecules bearing *N*-heterocyclic moieties, continue to represent a promising and adaptable class of organic compounds for developing next-generation antibacterial and antifungal agents. As a continuation of the search for biologically active hydrazone compounds with 5-oxopyrrolidine and diphenylamine fragments [29,30], we report the synthesis of 5-oxo-1-(4-(phenylamino)phenyl)pyrrolidine hydrazones bearing azole moieties and ADMET prediction of their biological properties.

2. Materials and Methods

2.1. Synthesis

Reagents were purchased from Sigma-Aldrich (St. Louis, MO, USA) and TCI Europe N.V. (Zwijndrecht, Belgium). The reaction course and purity of the synthesized compounds were monitored by TLC using aluminium plates precoated with silica gel 60 F254 (MerckKGaA, Darmstadt, Germany). The melting points were determined on a MEL-TEMP (Electrothermal, A Bibby Scientific Company, Burlington, NJ, USA) melting point apparatus and are uncorrected. The ^{1}H and ^{13}C NMR spectra were recorded in DMSO-d_6 on a Bruker Avance III (400 MHz, 101 MHz) spectrometer (Bruker BioSpin AG, Fällanden, Switzerland) operating in the Fourier transform mode. Chemical shifts (δ) are reported in parts per million (ppm) calibrated from TMS (0 ppm) as an internal standard for ^{1}H NMR, and DMSO-d_6 (39.43 ppm) for ^{13}C NMR. In ^{1}H NMR spectra, signal splitting is denoted using standard abbreviations: singlet (s), doublet (d), triplet (t), quartet (q), and multiplet (m). FT-IR spectra (ν, cm^{-1}) were recorded on a Perkin–Elmer Spectrum BX FT–IR spectrometer (Perkin–Elmer Inc., Waltham, MA, USA) using KBr pellets. Mass spectra were obtained on a Bruker maXis UHR-TOF mass spectrometer (Bruker Daltonics, Bremen, Germany) using ESI in both positive and negative ionization modes. Elemental analysis (C, H, N) were performed using the CE-440 Elemental Analyzer (Exeter Analytical, Inc., North Chelmsford, MA, USA).

*5-Oxo-1-(4-(phenylamino)phenyl)pyrrolidine-3-carbohydrazide (***1***)* was synthesized as described in [31]. M.p., ^{1}H and ^{13}C NMR spectra were found to be identical with the ones described in [31].

General procedure for the synthesis of compounds **2–4**

To hydrazide **1** (0.2 g, 0.65 mmol) dissolved in methanol (25 mL), a corresponding aldehyde (0.75 mmol) was added followed by addition of concentrated HCl (5 drops). The reaction mixture was stirred at 90 °C for 24 h. The precipitate formed was filtered off, dried and recrystallised from methanol and water mixture.

*5-Oxo-N′-((3-phenyl-1H-pyrazol-4-yl)methylene)-1-(4-(phenylamino)phenyl)pyrrolidine-3-carbohydrazide (***2***)*

Prepared from 3-phenyl-1*H*-pyrazole-4-carboxaldehyde. Yield 75% (0.23 g), green crystals; m.p. 122–123 °C. IR (KBr) ν_{max} (cm^{-1}): 1610, 1660 (C=O), 3100, 3310, 3614 (NH); ^{1}H NMR (400 MHz, DMSO-d_6): δ = 2.62–2.79 (m, 2H, H_{14}), 2.98–3.03 (m, 1H, H_{15}), 3.25–3.33 (m, 2H, H_{16}), 6.97–7.07 (m, 2H, $H_{9,11}$); 7.20 (t, 1H; J = 7.2 Hz, H_4); 7.35–7.41 (m, 2H, $H_{2,6}$); 7.66–7.68 (m, 5H, $H_{3,5,8,12,26}$); 7.73 (s, 1H, H_{24}); 7.75–7.78 (m, 2H; $H_{23,27}$); 7.80 (s,

1H, NH), 8.15 (s, 1H, H_{20}); 8.34 (s, 1H, H_{18}); 8.68 (s, 1H, H_{25}); 8.89 (s, 1H, NH); 9.87 (s, 1H, NH); ^{13}C NMR (101 MHz, DMSO-d_6): δ = 35.2 (C_{15}), 35.3, 36.0 (C_{14}), 51.0, 51.5 (C_{16}), 111.7, 112.3, 112.4, 116.7, 117.5, 120.0, 120.9, 121.2, 121.7, 122.2, 123.1, 124.3, 124.6, 129.6, 130.8, 130.9, 131.9, 137.3, 137.4, 140.4, 142.0, 143.9, 144.9, 168.5 ($C_{1–12,18,19–27}$), 172.0 (C_{13}); 172.3 (C_{17}); MS (ESI-): *m*/*z* calcd for $C_{27}H_{24}N_6O_2$, 463 [M-H]+; found 463. Anal. Calcd. for $C_{27}H_{24}N_6O_2$: C 69.81; H 5.21; N 18.09%; Found: C 69.79; H 5.19; N 18.05%.

N′-((1-methyl-1H-pyrazol-5-yl)methylene)-5-oxo-1-(4-(phenylamino)phenyl)pyrrolidine-3-carbohydrazide (**3**)

Prepared from 1-methyl-1*H*-pyrazole-5-carbaldehyde. Yield 68% (0.18 g), green crystals; m.p. 99–100 °C. IR (KBr) ν_{max} (cm^{-1}): 1612, 1660 (C=O), 3060, 3310, 3614 (NH); ^{1}H NMR (400 MHz, DMSO-d_6): δ = 2.66–2.81 (m, 2H; H_{14}); 3.38–3.48 (m, 1H, H_{15}); 3.90–4.04 (m, 2H, H_{16}); 3.67 (s, 3H, H_{22}); 5.42, 5.71 (2 s, 0.6H, NH); 6.77–6.81 (m, 1H, H_4); 7.00 (s, 2H, $H_{20,21}$); 7.02–7.12 (m, 4H, $H_{2,6,8,12}$); 7.19–7.29 (m, 2H, $H_{3,5}$); 7.29 (s, 0.4H, NH); 7.43–7.52 (m, 3H, $H_{9,11,18}$); 8.14 (s, 1H, NH); ^{13}C NMR (101 MHz, DMSO-d_6): δ = 35.0 (C_{15}); 35.2 (C_{14}); 50.3, 52.4 (C_{16}); 106.3 ($C_{20,21}$); 116.5 ($C_{2,6}$); 117.2; 117.3 ($C_{8,12}$); 119.7 (C_4); 121.5 (C_{10}); 129.3, 129.4 ($C_{3,5}$); 131.6, 131.7 ($C_{9,11}$); 133.3 (C_{19}); 140.2 (C_7), 143.7 (C_1); 171.2 (C_{13}); 173.5 (C_{17}); Anal. Calcd. for $C_{22}H_{22}N_6O_2$: C 65.66; H 5.51; N 20.88%; Found: C 65.59; H 5.53; N 20.81%.

N′-((1H-indol-4-yl)methylene)-5-oxo-1-(4-(phenylamino)phenyl)pyrrolidine-3-carbohydrazide (**4**)

Prepared from indole-4-carboxaldehyde. Yield 79% (0.22 g), light grey crystals; m.p. 200–201 °C. IR (KBr) ν_{max} (cm^{-1}): 1615, 1660 (C=O), 3050, 3310, 3615 (NH); ^{1}H NMR (400 MHz, DMSO-d_6): δ = 2.71–2.92 (m, 2H, H_{14}), 3.28–3.34 (m, 0.6H, H_{15}), 3.92–3.96 (m, 0.4H, H_{15}), 3.98–4.22 (m, 2H, H_{16}), 6.76–6.80 (m, 1H, H_4), 6.97–7.10 (m, 4H, $H_{8,12,24,25}$); 7.12–7.21 (m, 4H, $H_{2,3,5,6}$); 7.43–7.46 (m, 1H, H_{21}); 7.50 (d, 2H; *J* = 8.8 Hz, $H_{9,11}$); 7.77 (s, 1H, NH), 8.13 (s, 1H, $H_{20\ Indole}$); 8.14 (s, 0.6H, H_{18}); 8.21–8.24 (m, 1H, H_{22}); 8.38 (s, 0.4H, H_{18}); 11.20 (s, 0.6H, NH); 11.33 (s, 0.4H, NH); 11.57 (s, 1H, NH_{indole}); ^{13}C NMR (101 MHz, DMSO-d_6): δ = 33.1 (C_{15}), 35.0, 35.1, 35.8 (C_{14}), 50.8, 51.2 (C_{16}), 111.6, 112.1, 112.2, 116.4, 117.4, 119.7, 120.7, 121.0, 121.4, 122.1, 122.9, 124.2, 124.5, 129.4, 130.6, 130.8, 131.9, 132, 137.2, 137.3, 140.1, 141.6, 143.8, 144.5, 168.2 ($C_{1–12,18,19–26}$), 171.7 (C_{13}); 171.9, 173.1 (C_{17}); MS (ESI-): *m*/*z* calcd for $C_{26}H_{23}N_5O_2$, 436 [M-H]+; found 436. Anal. Calcd. for $C_{26}H_{23}N_5O_2$: C 71.38; H 5.30; N 16.01%; Found: C 71.32; H 5.23; N 15.95%.

N-(2,5-dimethyl-1H-pyrrol-1-yl)-5-oxo-1-(4-(phenylamino)phenyl)pyrrolidine-3-carboxamide (**5**)

A mixture of **1** (0.2 g, 0.65 mmol), propan-2-ol (10 mL), hexane-2,5-dione (0.08 g, 0.7 mmol), and acetic acid (1.5 mL) was refluxed for 5 h. Then cold water (20 mL) was added. The precipitate formed was filtered off and recrystallized from ethanol. Yield 86% (0.22 g), light grey crystals; m.p. 123–124 °C. IR (KBr) ν_{max} (cm^{-1}): 1644, 1678 (C=O), 3050, 3390 (NH); ^{1}H NMR (400 MHz, DMSO-d_6): δ = 2.00 (s, 6H, $H_{22,23}$); 2.68–2.74 (m, 1H; H_{14}); 2.83–2.89 (m, 1H; H_{14}); 3.42–3.50 (m, 1H, H_{15}); 3.92–3.96 (m, 1H, H_{16}); 4.10 (t, 1H, *J* = 9.2 Hz, H_{16}); 5.65 (s, 2H, $H_{19,20}$); 6.80 (t, 1H, *J* = 7.2 Hz, H_4); 7.03–7.10 (m, 4H, $H_{2,6,8,12}$); 7.22 (t, 2H, *J* = 8.0 Hz, $H_{3,5}$); 7.51 (d, 2H, *J* = 9.2 Hz, $H_{9,11}$); 8.15 (s, 1H, NH); 10.90 (s, 1H, NH); ^{13}C NMR (101 MHz, DMSO-d_6): δ = 10.9 ($C_{22,23}$); 34.1 (C_{15}); 35.4 (C_{14}); 50.7 (C_{16}); 103.1 ($C_{19,20}$); 116.3 ($C_{2,6}$); 117.2 ($C_{8,12}$); 119.4 (C_4); 121.2 ($C_{18,21}$); 126.7 (C_{10}); 129.2 ($C_{3,5}$); 131.6 ($C_{9,11}$); 140.0 (C_7), 143.6 (C_1); 170.9 (C_{13}); 172.0 (C_{17}); MS (ESI+): *m*/*z* calcd for $C_{23}H_{24}N_4O_2$, 389 [M+H]+; found 389. Anal. Calcd. for $C_{23}H_{24}N_4O_2$: C 71.11; H 6.23; N 14.42%; Found: C 71.10; H 6.19; N 14.39%.

2.2. In Silico Pharmacokinetics ADMET Study

The effectiveness and viability of drug molecules hinge on their pharmacodynamic and pharmacokinetic characteristics, which include vital aspects such as high therapeutic effectiveness, permissible toxicity levels, and selectivity for the target protein. This research utilized online platforms like ADMETlab 3.0 [32] and SwissADME [33] for assessing

drug-like properties and the ADMET (absorption, distribution, metabolism, excretion, and toxicity) profiles. The approach involved employing in silico predictions to evaluate intestinal absorption, penetration of the blood–brain barrier into the central nervous system, clearance, and potential toxicity of prospective drug candidates.

3. Results and Discussion

3.1. Chemistry

The hydrazone bond is formed through the condensation reaction of a hydrazine derivative with a carbonyl compound (aldehyde or ketone). The rate of formation of the hydrazone bond can be modulated by the electronic properties of the substituents on both the carbonyl and hydrazine moieties. For instance, aromatic hydrazones tend to be more stable than their aliphatic counterparts due to resonance stabilization. Incorporating pyrazole, pyrrole, or indole rings into hydrazone derivatives enhances antimicrobial activity, as these heterocyclic moieties increase the compounds' ability to interact with bacterial and fungal targets, often leading to improved efficacy against a broad spectrum of microorganisms. The presence of nitrogen-rich heterocycles in hydrazone scaffolds contributes to higher lipophilicity and better binding affinity to microbial enzymes, resulting in potent antibacterial and antifungal properties that surpass those of simple hydrazones [34–36]. Hydrazones **2**–**4** were synthesized according to the synthesis route reported previously [29,30]. Target hydrazones **2**–**4** were synthesized from 5-oxo-1-(4-(phenylamino)phenyl)pyrrolidine-3-carbohydrazide (**1**) [31] and the corresponding aldehydes in methanol at 90 °C in the presence of hydrochloric acid as a catalyst in 68–79% yield (Scheme 1). Though, the yields of all synthesized compounds are good, the slight differences are observed which can be explained by the differences in the structures of the target compounds. Hydrazone **4** bearing indole moiety, possesses a strongly conjugated system and, therefore, was obtained in the highest yield, whereas hydrazone **3** with methylpyrazole moiety gave the lowest yield due to insufficient resonance stabilization. These observations highlight the importance of electronic effects in hydrazone formation and suggest that modulation of substituent conjugation may serve as a useful strategy for improving synthetic efficiency in related systems.

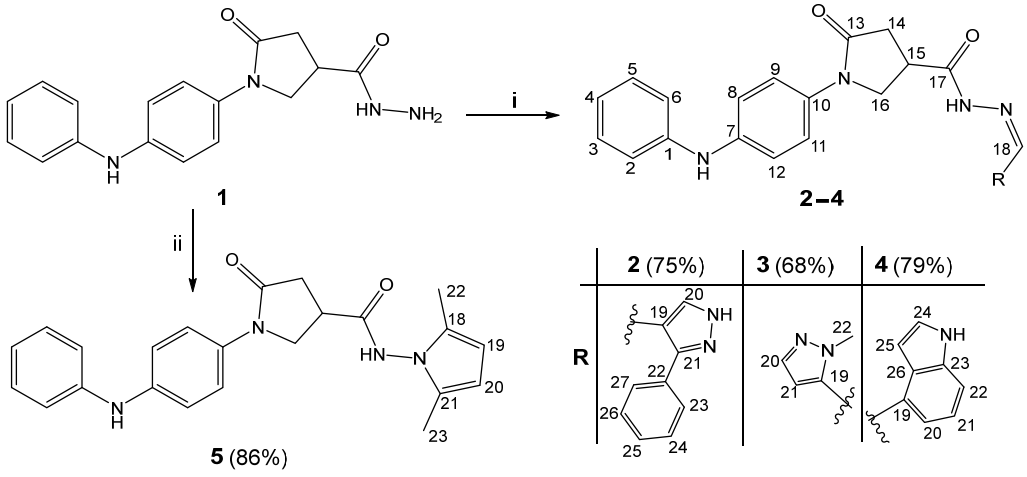

(i) RCHO, MeOH, reflux, 24 h; **(ii)** $CH_3CO(CH_2)_2COCH_3$, 2-PrOH, CH_3COOH, reflux, 5 h.

Scheme 1. Synthesis of compounds **2**–**5**.

Condensation reactions of acid hydrazides with aliphatic diketones provide five-membered heterocyclic compounds [37]. Thus, pyrrole derivative **5** was obtained from

hydrazide **1** in reaction with hexane-2,5-dione in acetic acid at reflux temperature of the reaction mixture. This reaction further demonstrates the synthetic versatility of the starting hydrazide and its suitability as a platform for generating structurally diverse heterocyclic frameworks, which could be exploited in future scaffold diversification studies.

The structures of the synthesized compounds **2**–**5** were confirmed by ^{1}H and ^{13}C NMR, IR, MS, and elemental analysis data. As an example, in the ^{1}H NMR spectrum for **2**, the formation of hydrazone linkage has been confirmed by the presence of a singlet at 8.34 ppm attributed to the proton in the N=CH group and a singlet at 8.89 ppm attributed to the amine proton in the CO-NH-N group. The NH proton in pyrazole ring resonated at 9.87 ppm. The evidence of the formation of pyrazole ring has been supported also by the singlet at 8.15 ppm attributed to the CH proton (H_{20}). The protons of the benzene ring originating from initial 3-phenyl-1*H*-pyrazole-4-carboxaldehyde gave additional peaks in the aromatic region of the spectrum. The assignments of aromatic protons and carbons were made based on ^{1}H and ^{13}C NMR data, chemical shift comparison with already published values [29], and characteristic splitting patterns. In the ^{1}H NMR spectrum of **3**, NH proton (H_{18}) of the N=CH group gave a set of resonances in the intensity ratio of 0.3:0.3:0.4 and, in the ^{1}H NMR spectrum of **4**, double sets of resonances of N=CH group proton (H_{18}) and CO-NH-N group proton in the intensity ratio 0.6:0.4 indicate the presence of a mixture of *Z*/*E* isomers resulting from the hindered rotation around the amide bond in DMSO-d_6 solutions. In the ^{1}H NMR spectra, the NH proton signals for the *Z* isomers appear more downfield than those observed for the corresponding protons in the *E* isomers [38]. No presence of *E*/*Z* isomers in the DMSO-d_6 solution is observed in the ^{1}H NMR spectra of **2** and **5**, since the possibility to observe *E* and *Z* isomers of hydrazones in DMSO-d_6 solution via ^{1}H NMR depends on the interplay of solvent polarity, intramolecular hydrogen bonding, and rate of interconversion. In many cases, only one isomer is detected or signals are averaged, because one isomer is heavily favored (e.g., by intramolecular hydrogen bonding or steric effects) or rapid interconversion between isomers averages them into a single set of signals [39]. The IR spectra of **2**–**4** show characteristic absorption bands at 1610–1615 cm^{-1} and 1660 cm^{-1} for the C=O group and ~3310–3615 cm^{-1} for NH stretching with additional peaks observed around and 3050–3100 cm^{-1}, indicating slight variations in their molecular environments. The formation of the 2,5-dimethylpyrrole moiety in compound **5** has been confirmed by the singlet at 2.00 ppm attributed to six protons of two methyl groups and the singlet at 5.65 ppm attributed to two protons in pyrrole ring in the ^{1}H NMR spectrum. The IR spectrum for **5** shows characteristic absorption bands at 1644 and 1678 cm^{-1} corresponding to C=O stretching vibrations, along with bands at 3050 and 3390 cm^{-1} attributable to NH stretching. Overall, the combined synthetic and spectroscopic results demonstrate that the investigated scaffold is both structurally adaptable and sensitive to electronic modulation, providing a valuable foundation for the rational design of new derivatives with improved properties.

3.2. Drug-Likeness Assessment and ADMET Predictions

The physicochemical and toxicity profiles of the four investigated compounds were evaluated within the established ADMET-guided framework for antimicrobial drug development in order to identify the candidate most likely to demonstrate favorable translational potential. Each compound was assessed with respect to molecular weight, lipophilicity, polarity, hydrogen bonding capacity, solubility, plasma protein binding, clearance, volume of distribution and predicted organ toxicity (Table 1) with emphasis on parameters known to indirectly support antimicrobial efficacy through improved permeability exposure and safety balance.

Table 1. ADMET properties of compounds **2**–**5**.

Compound	Biological Properties						
	log *P*	TPSA, Å^2	$T_{1/2}$, h	Plasma Protein Binding, %	BBB Penetration	Hepatotoxicity, %	Nephrotoxicity, %
2	3.768	102.48	0.714	96.2	No	92.6	89.8
3	2.661	91.62	0.745	98.0	No	89.8	95.4
4	3.592	89.59	0.635	90.4	No	92.6	94.3
5	2.589	66.37	0.510	96.7	Yes	90.2	85.3

One of the criteria of Lipinski's RO5, the primary method in determining if a compound is suitable as a drug-like molecule, is a log *P* value, which should be less than 5. Molecular lipophilicity, commonly quantified by the octanol–water partition coefficient (expressed as log *P* for neutral molecules), is a key physicochemical parameter influencing a compound's bioavailability and serves as a valuable indicator for predicting its permeability in biological systems [40]. All synthesized compounds **2**–**4** meet this criterion. Additionally, the Pfizer 3/75 rule states that compounds with a log *P* value greater than 3 and a topological polar surface area (TPSA) less than 75 Å^2 are more likely to be toxic [41]. Compounds **2**, **4** (log *P* > 3) and **5** (TPSA < 75 Å^2) have partially complied with the Pfizer rule; however, this rule is not as frequently considered as the Lipinski's rule, and all synthesized compounds fall within the TPSA range (20–130 Å^2) that determines good oral bioavailability.

Molecular weight constitutes one of the primary determinants influencing bacterial penetration and systemic drug behaviour. For small-molecule antibacterial agents, a molecular weight range between approximately 250 and 600 Da is generally considered favourable, with an optimal range of 300 to 500 Da often associated with enhanced permeability. Compounds exceeding 600 Da typically display limited passive diffusion across bacterial membranes unless specific uptake mechanisms are present [42,43]. All synthesized compounds exhibited a molecular weight in the range of 388–464 Da, which falls within the generally acceptable antibacterial range and remains compatible with passive membrane diffusion.

Compounds bearing greater number of benzene ring fragments in their structure tend to have higher log *P* values and a greater likelihood of being hepatotoxic and nephrotoxic [44]. Thus, compound **2**, bearing phenyl-pyrazole moiety, and **4**, bearing indole moiety, have been predicted to have higher log *P* values, 3.768 and 3.592, respectively, which lie near the upper boundary of the preferred range (1–4), suggesting adequate membrane permeability but increased risk of elevated plasma protein binding and reduced solubility. Compounds **3** and **5** with log *P* values of 2.661 and 2.589, respectively, are more optimal and lie comfortably within the preferred range.

The topological polar surface area (TPSA) values of compounds **2**, **3** and **4** (89.59–102.48 Å^2) are slightly above the optimal threshold often associated with efficient permeation, though still within the broader acceptable range for antibacterial agents [45]. TPSA value of compound **5** (66.37 Å^2) lies comfortably within the range associated with efficient bacterial membrane crossing and is the lowest among synthesized compounds, thereby suggesting superior permeability potential. Judging by these two indicators, log *P* and TPSA, compound **3** has been predicted to be the best candidate for being a potential drug-like molecule.

Hydrogen bond donor (HBD) and acceptor (HBA) counts for all synthesized compounds have remained within recommended limits, promoting permeability efficiency. Hydrogen bonding capacity plays a critical role in membrane permeability. Limiting hydrogen bond donors to five or fewer and hydrogen bond acceptors to ten or fewer supports favourable diffusion characteristics, as excessive hydrogen bonding potential increases

polarity and reduces membrane transit efficiency [46]. HBD of the synthesized compounds lies within the range of 2–3, while HBA ranges from 2 to 4, well within the preferred range.

Aqueous solubility remains an essential parameter, as insufficient solubility often limits the attainment of therapeutic concentrations in vivo [47]. The typical log *S* range of −1 to −5 observed for many pharmaceuticals represents a balance between sufficient polarity to maintain aqueous solubility and enough hydrophobic character to enable effective membrane permeability [48]. Predicted aqueous solubility (log *S*) values of compounds **2** and **4**, −5.786 and −5.798, respectively, are markedly poor, indicating poor solubility, which may limit achievable systemic concentrations, suggesting limited systemic exposure. Log *S* value of compound **3** (−4.322) has improved relative to compounds **2** and **4**, though still approaching the lower acceptable boundary. Compound **5** demonstrated the most favourable solubility profile with a log *S* value of −3.881, indicating improved aqueous behaviour relative to other synthesized compounds and enhancing the likelihood of achieving therapeutic concentrations.

All synthesized compounds have been predicted to have good absorption in the gastrointestinal tract, but not all have been predicted to cross the blood–brain barrier. There are two main indicators which predict if a compound is able to penetrate the blood–brain barrier—log *P* value range of 0.5–6 and TPSA value of <80 $Å^2$ [33]. Compounds **2** (phenyl-pyrazole derivative) and **4** (indole derivative) have been predicted to have higher TPSA values, which result in more difficult penetration of the blood–brain barrier. Compound **5** (pyrrole derivative) is the only compound that has been predicted to be able to cross this barrier. Blood–brain barrier permeability may be advantageous for the treatment of central nervous system infections but is unnecessary for many systemic infections and may increase the risk of central nervous system adverse effects [49].

All synthesized compounds have been predicted to have a short half-life ($T_{1/2}$). This indicator determines the compounds' rapid metabolism and excretion [50]. Predicted short half-lives indicate that synthesized compounds would receive insufficient exposure, requiring high and/or frequent dosing. The longest half-life (0.745 h) was calculated for pyrazole derivative **3**. The half-lives of all other synthesized compounds have been predicted to be in the range of 0.510–0.714 h.

Clearance (CL) is defined as the theoretical volume of plasma from which a drug is completely removed per unit time, representing the combined efficiency of elimination pathways such as hepatic metabolism and renal excretion [51]. In the present case, all four newly synthesized compounds exhibited low-to-moderate clearance (3.068–5.577 mL/min/kg) alongside short half-lives. Given this relationship, a short $T_{1/2}$ despite relatively low CL suggests that the volume of distribution (V_d) of all synthesized compounds is also predicted to have low values. The aforementioned parameter, which characterizes the extent of drug distribution beyond the systemic circulation [52], could not be calculated using the selected pharmacokinetic model. Collectively, these findings indicate that the compounds are likely confined largely to the plasma with limited tissue distribution. Furthermore, the data underscores that more complex modeling approaches are required in order to accurately describe their pharmacokinetic profiles, parameter interrelationships and influence on dosing regimens and therapeutic potential.

The percentage of a molecule that binds to blood plasma proteins is an indicator which determines its therapeutic index. The therapeutic index is an indicator of the safety of a drug molecule. Compounds with a plasma protein binding (PPB) of more than 90% are predicted to have a low therapeutic index, which would make them difficult to utilize in medicine [32,53]. Compounds **2**–**5** have been predicted to have a low therapeutic index, with their PPB predicted to be in the range of 90.4–98.0%. The indole derivative **4** has been predicted to have the lowest PPB of 90.4%. This pharmacokinetic property increases the

compound's likelihood of being a drug-like molecule compared to the other compounds analyzed in this study.

When integrating all ADMET-related determinants including molecular weight, lipophilicity, polarity, hydrogen bonding, solubility, plasma protein binding, and predicted organ toxicity, pyrrole derivative **5** has demonstrated the most balanced overall profile. It satisfies the principal physicochemical criteria associated with antimicrobial activity and shows the most acceptable solubility while presenting comparatively lower predicted hepatotoxicity and nephrotoxicity risks. Although plasma protein binding remains elevated across all synthesized compounds, compound **5** offers the most favourable compromise between permeability, exposure and safety considerations.

Importantly, these findings identify clear directions for future optimization, including structural modifications aimed at improving solubility, reducing plasma protein binding, and enhancing metabolic stability. Approaches such as targeted functional group modification, bioisosteric replacement, or prodrug strategies may further improve the pharmacokinetic profiles of this compound class. Taken together, the present study establishes a promising framework for further structure-activity relationship (SAR) investigations and supports continued development of hydrazone-based derivatives as potential antimicrobial agents. Future work should focus on biological evaluation and systematic structural optimization to convert these physicochemical advantages into measurable biological activity.

3.3. ADMET Profile Comparison to Commercial Hydrazone Agents

To assess the relevance of the ADMET predictions obtained in this study, the results were benchmarked against the ADMET profiles of biologically active hydrazine–hydrazone derivatives reported in clinical use. For this purpose, key ADMET parameters of established therapeutic agents, including nifuroxazide, furazolidone, nitrofurazone and nifuratel (Supplementary Material, Figure S11), were calculated (Table 2) and directly compared with those of the newly synthesized compounds **2–5** [54,55].

Table 2. ADMET properties of commercial hydrazone agents.

Compound	Biological Properties						
	log *P*	**TPSA, Å^2**	**$T_{1/2}$, h**	**Plasma Protein Binding, %**	**BBB Penetration**	**Hepatotoxicity, %**	**Nephrotoxicity, %**
Nifuroxazide	1.055	120.65	0.931	96.3	No	7.1	0.8
Furazolidone	−0.362	100.86	1.758	54.5	No	17.1	23.1
Nitrofurazone	−0.291	126.44	1.309	75.5	No	17.7	3.7
Nifuratel	0.393	126.16	0.923	76.3	No	51.6	56.5

All selected commercially available hydrazone-based therapeutics comply fully with Lipinski's RO5 and the Pfizer 3/75 rule, with no observed violations. Compared to compounds **2–5**, these reference drugs exhibit lower lipophilicity, with log *P* values ranging from −0.362 for furazolidone to 1.055 for nifuroxazide, suggesting reduced membrane permeability, limited accumulation in lipid-rich tissues, and a greater preference for aqueous environments.

The topological polar surface area (TPSA) values of these compounds fall within 100.86–126.44 Å^2, exceeding those of compounds **2–5** and slightly surpassing the threshold typically associated with optimal passive permeability, yet remaining within acceptable limits for antimicrobial agents. Variations in hydrogen bonding capacity were also evident: the commercial hydrazones possess 0–2 hydrogen bond donors (HBD) and 5–6 hydrogen bond acceptors (HBA), indicating lower donor counts but higher acceptor capacity relative to the newly synthesized derivatives. This balance supports favorable interactions

with aqueous and polar environments while potentially limiting passive diffusion across lipid membranes.

In terms of solubility, calculated log *S* values range from −4.085 for nifuroxazide to −3.157 for furazolidone, exceeding those of compounds **2**–**5** and reflecting improved aqueous solubility alongside a balanced polarity-lipophilicity profile. Furthermore, all evaluated reference compounds demonstrate high predicted gastrointestinal absorption while lacking permeability across the blood–brain barrier, thereby reducing the likelihood of central nervous system-related adverse effects.

The evaluated reference hydrazones generally exhibited lower plasma protein binding (PPB) values (54.5–76.3%) compared to compounds **2**–**5**, with the exception of nifuroxazide (96.3%). These observations suggest that, although reduced PPB is often associated with improved safety profiles, values exceeding 90% do not necessarily preclude a compound from being safe and therapeutically effective. Toxicity predictions further indicated that nifuroxazide, furazolidone, and nitrofurazone possess substantially lower risks of hepatotoxicity and nephrotoxicity (<25%) relative to compounds **2**–**5**, potentially reflecting structural differences such as a reduced number of phenyl moieties.

In contrast, nifuratel demonstrated higher predicted probabilities of hepatotoxicity (51.6%) and nephrotoxicity (56.5%). Despite this, it is widely regarded as clinically safe, with minimal or negligible adverse effects reported in practice, underscoring the importance of subsequent in vivo validation for investigational compounds.

Pharmacokinetic analysis revealed that the commercial hydrazones exhibit longer half-life ($T_1/_2$ = 0.923–1.758 h) and higher clearance (CL = 2.920–6.021 mL/min/kg) values compared to compounds **2**–**5**, with only nitrofurazone showing a slightly lower clearance (2.920 mL/min/kg). The combination of increased half-life and clearance suggests a greater apparent volume of distribution, indicating that these compounds are more extensively distributed beyond systemic circulation and may reach their biological targets more effectively.

As a result, future investigations should prioritize comprehensive biological evaluation conducted alongside systematic structural optimization in order to translate favorable physicochemical properties into favorable biological activity. In this context, rational modification of functional groups represents a viable strategy for improving the pharmacokinetic characteristics of this compound class. Overall, the present comparisons highlight key avenues for further optimization, particularly through structural adjustments directed at reducing plasma protein binding, improving metabolic stability and enhancing aqueous solubility.

4. Conclusions

In summary, hydrazone derivatives, bearing selected azole moieties **2**–**5,** were successfully synthesized from 5-oxo-1-(4-(phenylamino)phenyl)pyrrolidine-3-carbohydrazide using straightforward and efficient synthetic procedures, in good yields (68–79%). Structural elucidation by spectroscopic methods (^{1}H and ^{13}C NMR, IR, MS, and elemental analysis) confirmed the formation of the desired products and provided insight into their configurational behavior, including the presence or absence of E/Z isomerism depending on intramolecular interactions and dynamic processes in DMSO-d_6 solution.

Drug-likeness and ADMET evaluation revealed that all synthesized compounds fall within generally acceptable physicochemical ranges for small-molecule antibacterial agents, although differences in lipophilicity, polarity, and solubility were observed. Among the investigated compounds, the pyrrole derivative **5** demonstrated the most balanced pharmacokinetic profile, combining favorable lipophilicity, optimal polarity (TPSA), and the best predicted aqueous solubility, along with comparatively lower toxicity risks. Compound **5**

has been identified as the most promising candidate for further optimization and in vivo biological evaluation.

Supplementary Materials: The following supporting information can be downloaded at: https://www.mdpi.com/article/10.3390/org7020020/s1, Figure S1. ^{1}H NMR Spectrum of **2** (DMSO-d_6, 400 MHz); Figure S2. ^{13}C NMR Spectrum of **2** (DMSO-d_6, 101 MHz); Figure S3. MS spectrum of **2**; Figure S4. ^{1}H NMR Spectrum of **3** (DMSO-d_6, 400 MHz); Figure S5. ^{13}C NMR Spectrum of **3** (DMSO-d_6, 101 MHz); Figure S6. ^{1}H NMR Spectrum of **4** (DMSO-d_6, 400 MHz); Figure S7. ^{13}C NMR Spectrum of **4** (DMSO-d_6, 101 MHz); Figure S8. MS spectrum of **4**; Figure S9. ^{1}H NMR Spectrum of **5** (DMSO-d_6, 400 MHz); Figure S10. ^{13}C NMR Spectrum of **5** (DMSO-d_6, 101 MHz); Figure S11. MS spectrum of **5**; Figure S12. Commercial therapeutic agents, bearing hydrazone moiety.

Author Contributions: Conceptualization, K.K. and I.T.; methodology, I.J. and I.T.; formal analysis, J.K., K.K., I.J. and I.T.; investigation, J.K. and I.T.; resources, K.K. and I.T.; writing—original draft preparation, J.K., K.K. and I.T.; writing—review and editing, J.K., K.K., I.J. and I.T.; visualization, J.K. and I.T.; supervision, K.K. and I.T.; project administration, K.K.; funding acquisition, K.K. and I.T. All authors have read and agreed to the published version of the manuscript.

Funding: This research has received funding from the Research Council of Lithuania (LMTLT), agreement No S-SV-24-173.

Data Availability Statement: The original contributions presented in this study are included in the article/Supplementary Material. Further inquiries can be directed to the corresponding author.

Conflicts of Interest: The authors declare no conflicts of interest.

References

1. Suruchi; Tiwari, M.; Pal, D.; Gupta, A.K.; Jain, S.K. Breaking Barriers in Antimicrobial Therapy: Resistance Mechanisms and Novel Antimicrobial Strategies. *Microb. Pathog.* **2026**, *210*, 108163. [CrossRef] [PubMed]
2. Murray, C.J.L.; Ikuta, K.S.; Sharara, F.; Swetschinski, L.; Robles Aguilar, G.; Gray, A.; Han, C.; Bisignano, C.; Rao, P.; Wool, E.; et al. Global Burden of Bacterial Antimicrobial Resistance in 2019: A Systematic Analysis. *Lancet* **2022**, *399*, 629–655. [CrossRef] [PubMed]
3. Kaspute, G.; Zebrauskas, A.; Streckyte, A.; Ivaskiene, T.; Prentice, U. Combining Advanced Therapies with Alternative Treatments: A New Approach to Managing Antimicrobial Resistance? *Pharmaceutics* **2025**, *17*, 648. [CrossRef]
4. DrugBank Online. Isoniazid. Available online: https://go.drugbank.com/drugs/DB00951 (accessed on 30 January 2026).
5. DrugBank Online. Nifuroxazide. Available online: https://go.drugbank.com/drugs/DB13855 (accessed on 30 January 2026).
6. Popiołek, Ł. Hydrazide–Hydrazones as Potential Antimicrobial Agents: Overview of the Literature since 2010. *Med. Chem. Res.* **2017**, *26*, 287–301. [CrossRef]
7. Rollas, S.; Küçükgüzel, S. Biological Activities of Hydrazone Derivatives. *Molecules* **2007**, *12*, 1910–1939. [CrossRef]
8. Thorat, B.R.; Mali, S.N.; Shah, U.; Garg, A.; Agrawal, R.; Arvindekar, S.A.; Cruz, J.N.; de Oliveira, M.S.; Shaik, A.B.; Lokesh, B.V.S. Hydrazide-Hydrazone Derivatives and Their Antitubercular Activity. *Russ. J. Bioorg. Chem.* **2025**, *51*, 35–52. [CrossRef]
9. Atta-ur-Rahman (Ed.) *Frontiers in Clinical Drug Research-Anti Infectives*; Bentham Science Publishers: Sharjah, United Arab Emirates, 2024; Volume 9.
10. Verma, G.; Marella, A.; Shaquiquzzaman, M.; Akhtar, M.; Ali, M.; Alam, M. A Review Exploring Biological Activities of Hydrazones. *J. Pharm. Bioallied Sci.* **2014**, *6*, 69. [CrossRef]
11. Czyżewska, I.; Mazur, L.; Popiołek, Ł. Transition Metal Complexes of Hydrazones as Potential Antimicrobial and Anticancer Agents: A Short Review. *Chem. Biol. Drug Des.* **2024**, *104*, e14590. [CrossRef] [PubMed]
12. Zülfikaroğlu, A.; Yüksektepe Ataol, Ç.; Çelikoğlu, E.; Çelikoğlu, U.; İdil, Ö. New Cu(II), Co(III) and Ni(II) Metal Complexes Based on ONO Donor Tridentate Hydrazone: Synthesis, Structural Characterization, and Investigation of Some Biological Properties. *J. Mol. Struct.* **2020**, *1199*, 127012. [CrossRef]
13. Popiołek, Ł. Updated Information on Antimicrobial Activity of Hydrazide–Hydrazones. *Int. J. Mol. Sci.* **2021**, *22*, 9389. [CrossRef]
14. Arora, T.; Devi, J.; Boora, A.; Taxak, B.; Rani, S. Synthesis and Characterization of Hydrazones and Their Transition Metal Complexes: Antimicrobial, Antituberculosis and Antioxidant Activity. *Res. Chem. Intermed.* **2023**, *49*, 4819–4843. [CrossRef]
15. Tafere, D.A.; Gebrezgiabher, M.; Elemo, F.; Sani, T.; Atisme, T.B.; Ashebr, T.G.; Ahmed, I.N. Hydrazones, Hydrazones-Based Coinage Metal Complexes, and Their Biological Applications. *RSC Adv.* **2025**, *15*, 6191–6207. [CrossRef] [PubMed]

16. Shah, K.; Gupta, J.K.; Chauhan, N.S.; Upmanyu, N.; Shrivastava, S.K.; Mishra, P. Prodrugs of NSAIDs: A Review. *Open Med. Chem. J.* **2017**, *11*, 146–195. [CrossRef]
17. Teneva, Y.; Simeonova, R.; Valcheva, V.; Angelova, V.T. Recent Advances in Anti-Tuberculosis Drug Discovery Based on Hydrazide–Hydrazone and Thiadiazole Derivatives Targeting InhA. *Pharmaceuticals* **2023**, *16*, 484. [CrossRef]
18. Poyraz, S.; Döndaş, H.A.; Döndaş, N.Y.; Sansano, J.M. Recent Insights about Pyrrolidine Core Skeletons in Pharmacology. *Front. Pharmacol.* **2023**, *14*, 1239658. [CrossRef]
19. Cusumano, A.Q.; Pierce, J.G. 3-Hydroxy-1,5-Dihydro-2H-Pyrrol-2-Ones as Novel Antibacterial Scaffolds against Methicillin-Resistant *Staphylococcus aureus*. *Bioorg. Med. Chem. Lett.* **2018**, *28*, 2732–2735. [CrossRef]
20. Ohta, K.; Chiba, Y.; Kaise, A.; Endo, Y. Structure–Activity Relationship Study of Diphenylamine-Based Estrogen Receptor (ER) Antagonists. *Bioorg. Med. Chem.* **2015**, *23*, 861–867. [CrossRef]
21. Kumar, A.; Mishra, A.K. Pharmacological Applications of Diphenylamine and Its Derivative as Potent Bioactive Compound: A Review. *Curr. Bioact. Compd.* **2018**, *14*, 217–233. [CrossRef]
22. Shah, A.; Desai, K.; Bhanusali, A.; Agrawal, S.; Patel, K.; Naik, N.; Thakar, A.; Naik, H.; Kanjariya, D.; Malek, N.; et al. In Vitro and In Silico Evaluation of Fluorinated Diphenylamine Chalcone Derivatives as Potential Antimalarial and Anticancer Agents. *Sci. Rep.* **2025**, *15*, 18928. [CrossRef]
23. Kumar, A.; Mishra, A. Synthesis and Antimicrobial Activity of Some New Diphenylamine Derivatives. *J. Pharm. Bioallied Sci.* **2015**, *7*, 81. [CrossRef] [PubMed]
24. Poyraz, S.; Canacankatan, N.; Belveren, S.; Yetkin, D.; Kibar, K.; Ülger, M.; Sansano, J.M.; Özcelik, N.D.; Necat Yılmaz, Ş.; Döndaş, H.A. Study of the Anti(Myco)Bacterial and Antitumor Activities of Prolinate and N-Amidocarbothiolprolinate Derivatives Based on Fused Tetrahydropyrrolo[3,4-c]Pyrrole-1,3(2H,3aH)-Dione, Bearing an Indole Ring. *Monatshefte Chem.-Chem. Mon.* **2018**, *149*, 2253–2263. [CrossRef]
25. Chauhan, S.; Verma, V.; Kumar, D.; Gupta, R.; Gupta, S.; Bajaj, A.; Kumar, A.; Parshad, M. N-Heterocycles Hybrids: Synthesis, Antifungal and Antibiofilm Evaluation. *Synth. Commun.* **2022**, *52*, 898–911. [CrossRef]
26. Periwal, P.; Verma, V.; Kumar, D.; Kumar, A.; Bhatia, M.; Thakur, S.; Parshad, M. Novel Azole–Sulfonamide Conjugates as Potential Antimicrobial Candidates: Synthesis and Biological Assessment. *Future Med. Chem.* **2024**, *16*, 157–171. [CrossRef] [PubMed]
27. Mehta, D.K.; Chaurasiya, R.; Das, R. Recent Developments in Azetidinone-Azole Conjugates: Emerging Antimicrobial Potentials. *Med. Chem.* **2025**, *21*, 761–771. [CrossRef]
28. Guan, L.; Yang, H.; Cai, Y.; Sun, L.; Di, P.; Li, W.; Liu, G.; Tang, Y. ADMET-Score—A Comprehensive Scoring Function for Evaluation of Chemical Drug-Likeness. *MedChemComm* **2019**, *10*, 148–157. [CrossRef]
29. Zubrickė, I.; Jonuškienė, I.; Kantminienė, K.; Tumosienė, I.; Petrikaitė, V. Synthesis and In Vitro Evaluation as Potential Anticancer and Antioxidant Agents of Diphenylamine-Pyrrolidin-2-One-Hydrazone Derivatives. *Int. J. Mol. Sci.* **2023**, *24*, 16804. [CrossRef]
30. Tumosienė, I.; Stasevych, M.; Zvarych, V.; Jonuškienė, I.; Kantminienė, K.; Petrikaitė, V. Novel 5-Oxopyrrolidine-3-Carbohydrazides as Potent Protein Kinase Inhibitors: Synthesis, Anticancer Evaluation, and Molecular Modeling. *Int. J. Mol. Sci.* **2025**, *26*, 3162. [CrossRef]
31. Tumosienė, I.; Jonuškienė, I.; Kantminienė, K.; Mickevičius, V.; Petrikaitė, V. Novel N-Substituted Amino Acid Hydrazone-Isatin Derivatives: Synthesis, Antioxidant Activity, and Anticancer Activity in 2D and 3D Models In Vitro. *Int. J. Mol. Sci.* **2021**, *22*, 7799. [CrossRef]
32. Fu, L.; Shi, S.; Yi, J.; Wang, N.; He, Y.; Wu, Z.; Peng, J.; Deng, Y.; Wang, W.; Wu, C.; et al. ADMETlab 3.0: An Updated Comprehensive Online ADMET Prediction Platform Enhanced with Broader Coverage, Improved Performance, API Functionality and Decision Support. *Nucleic Acids Res.* **2024**, *52*, W422–W431. [CrossRef]
33. Daina, A.; Michielin, O.; Zoete, V. SwissADME: A Free Web Tool to Evaluate Pharmacokinetics, Drug-Likeness and Medicinal Chemistry Friendliness of Small Molecules. *Sci. Rep.* **2017**, *7*, 42717. [CrossRef] [PubMed]
34. Rawat, P.; Bharati, P.; Gautam, A.; Kumar, M.; Singh, R.; Prakash; Ram, A.; Gautam, S.; Darwari, A.; Mishra, A.; et al. Design and Synthesis of Pyrazole, Pyrazolone and 1,3,4-Oxadiazole Derivatives Having Pyrrole Motif as a Source of New Antimicrobial and Anticancer Agents. *J. Mol. Struct.* **2023**, *1272*, 134087. [CrossRef]
35. Rawat, P.; Singh, R.N.; Ranjan, A.; Ahmad, S.; Saxena, R. Antimycobacterial, Antimicrobial Activity, Experimental (FT-IR, FT-Raman, NMR, UV-Vis, DSC) and DFT (Transition State, Chemical Reactivity, NBO, NLO) Studies on Pyrrole-Isonicotinyl Hydrazone. *Spectrochim. Acta. Part A Mol. Biomol. Spectrosc.* **2017**, *179*, 1–10. [CrossRef] [PubMed]
36. Kumar, N.; Asija, S.; Deswal, Y.; Saroya, S.; Kumar, A.; Devi, J. Organotin(IV) Complexes Derived from Hydrazone Ligands: Synthesis, Spectral Analysis, Antimicrobial and Molecular Docking Studies. *Phosphorus Sulfur Silicon Relat. Elem.* **2022**, *197*, 952–963. [CrossRef]
37. Tumosienė, I.; Kantminienė, K.; Klevinskas, A.; Petrikaitė, V.; Jonuškienė, I.; Mickevičius, V. Antioxidant and Anticancer Activity of Novel Derivatives of 3-[(4-Methoxyphenyl)Amino]Propane-Hydrazide. *Molecules* **2020**, *25*, 2980. [CrossRef]

38. Tisovský, P.; Csicsai, K.; Donovalová, J.; Šandrik, R.; Sokolík, R.; Gáplovský, A. Effect of a =X-NH-Fragment, (X = C, N), on Z/E Isomerization and ON/OFF Functionality of Isatin Arylhydrazones, ((Arylamino)Methylene)Indolin-2-Ones and Their Anions. *Molecules* **2020**, *25*, 3082. [CrossRef] [PubMed]
39. Moradi Rufchahi, E.; Mirsadeghi, F.A. Solvatochromic, Computational Chemical and E/Z Geometrical Isomerism Studies on Some Aryl-Hydrazones Synthesised by Reacting of Aryldiazonium Chlorides with 6-Butyl-4-Hydroxyquinolin-2(1H)-One. *Color. Technol.* **2025**, *141*, 325–343. [CrossRef]
40. De La Fuente, M.; Folgar, R.M.; Martínez-Paz, P.; Cortés, E.; Martínez-Guitarte, J.L.; Morales, M. Effect of Environmental Stressors on the mRNA Expression of Ecdysone Cascade Genes in Chironomus Riparius. *Environ. Sci. Pollut. Res.* **2022**, *29*, 10210–10221. [CrossRef]
41. Khuzwayo, S.S.; Selepe, M.A.; Meyer, D.; Gama, N.H. The Synthesis and Investigation of Novel 3-Benzoylbenzofurans and Pyrazole Derivatives for Anti-HIV Activity. *RSC Med. Chem.* **2025**, *16*, 2142–2158. [CrossRef]
42. El Zahed, S.S.; French, S.; Farha, M.A.; Kumar, G.; Brown, E.D. Physicochemical and Structural Parameters Contributing to the Antibacterial Activity and Efflux Susceptibility of Small-Molecule Inhibitors of *Escherichia coli*. *Antimicrob. Agents Chemother.* **2021**, *65*, e01925-20. [CrossRef]
43. Ramirez, D.M.; Schweizer, F. Development of Polymyxin- and Aminoglycoside-Based Outer Membrane Permeabilizers: A Review. *Front. Microbiol.* **2025**, *16*, 1625300. [CrossRef]
44. Huang, H.-J.; Lee, Y.-H.; Chou, C.-L.; Zheng, C.-M.; Chiu, H.-W. Investigation of Potential Descriptors of Chemical Compounds on Prevention of Nephrotoxicity via QSAR Approach. *Comput. Struct. Biotechnol. J.* **2022**, *20*, 1876–1884. [CrossRef]
45. De Oliveira, E.C.L.; Da Costa, K.S.; Taube, P.S.; Lima, A.H.; Junior, C.D.S.D.S. Biological Membrane-Penetrating Peptides: Computational Prediction and Applications. *Front. Cell. Infect. Microbiol.* **2022**, *12*, 838259. [CrossRef]
46. Alex, A.; Millan, D.S.; Perez, M.; Wakenhut, F.; Whitlock, G.A. Intramolecular Hydrogen Bonding to Improve Membrane Permeability and Absorption in beyond Rule of Five Chemical Space. *MedChemComm* **2011**, *2*, 669. [CrossRef]
47. Elder, D.; Holm, R. Aqueous Solubility: Simple Predictive Methods (In Silico, In Vitro and Bio-Relevant Approaches). *Int. J. Pharm.* **2013**, *453*, 3–11. [CrossRef]
48. Jorgensen, W.L.; Duffy, E.M. Prediction of Drug Solubility from Structure. *Adv. Drug Deliv. Rev.* **2002**, *54*, 355–366. [CrossRef]
49. Haddad, N.; Carr, M.; Balian, S.; Lannin, J.; Kim, Y.; Toth, C.; Jarvis, J. The Blood–Brain Barrier and Pharmacokinetic/Pharmacodynamic Optimization of Antibiotics for the Treatment of Central Nervous System Infections in Adults. *Antibiotics* **2022**, *11*, 1843. [CrossRef]
50. Andrade, C. The Practical Importance of Half-Life in Psychopharmacology. *J. Clin. Psychiatry* **2022**, *83*, 41940. [CrossRef]
51. Schrag, M.; Regal, K. Chapter 3—Pharmacokinetics and Toxicokinetics. In *A Comprehensive Guide to Toxicology in Preclinical Drug Development*; Faqi, A.S., Ed.; Academic Press: Cambridge, MA, USA, 2013; pp. 31–68.
52. Johanson, G. 1.09—Toxicokinetics and Modeling. In *Comprehensive Toxicology*, 4th ed.; McQueen, C.A., Ed.; Elsevier: Oxford, UK, 2026; pp. 191–213.
53. Toma, C.; Gadaleta, D.; Roncaglioni, A.; Toropov, A.; Toropova, A.; Marzo, M.; Benfenati, E. QSAR Development for Plasma Protein Binding: Influence of the Ionization State. *Pharm. Res.* **2019**, *36*, 28. [CrossRef]
54. Deshmukh, H.S.; Adole, V.A.; Frit, A.A.P.; Mali, S.N.; Yasin, H.K.A.; Patil, B.N.; Janani, S.; Jagdale, B.S. Synthesis, Characterization, Computational and Biological Evaluation of Pyrazole Hydrazones as Promising Anti-Inflammatory Agents. *Sci. Rep.* **2025**, *15*, 42206. [CrossRef]
55. Santhosh, C.R.; Chinnam, S.; Ananthnag, G.S.; Oduselu, G.O.; Chidambaram, K.; Kerru, N.; Kottam, N.; Madhu, G.M. Design, Synthesis, Crystal Structure of Novel Hydrazone Analogues as SARS-CoV-2 Potent Inhibitors: MD Simulations, MM-GBSA, Docking and ADMET Studies. *R. Soc. Open Sci.* **2025**, *12*, 250373. [CrossRef]